Brain Ventricle Segmentation Combining Template-based Deformable Registration with Texture-based Fuzzy Connectedness and Shape-based Expectation-Maximization

John J. Drozd[1] PhD, Robert K. Moreland[1] MD, Samaneh Kazemifar[1,4] MSc, Michael Borrie[2,3] MB ChB, Robert Bartha[1,4] PhD, and for the Alzheimer's Disease Neuroimaging Initiative

[1]Robarts Research Institute, [2]Department of Medicine, [4]Department of Medical Biophysics, Schulich School of Medicine and Dentistry, Western University, P.O. Box 5015, 100 Perth Drive, London, ON, Canada N6A 5K8
[3]Division of Aging, Rehabilitation and Geriatric Care, Lawson Health Research Institute, 801 Commissioners Rd. E, London ON, Canada N6C 5J1

Data used in preparation of this article were obtained from the Alzheimer's Disease Neuroimaging Initiative (ADNI) database (adni.loni.ucla.edu). As such, the investigators within the ADNI contributed to the design and implementation of ADNI and/or provided data but did not participate in analysis or writing of this report. A complete listing of ADNI investigators can be found at:
http://adni.loni.ucla.edu/wp-content/uploads/how_to_apply/ADNI_Acknowledgement_List.pdf

Corresponding Author: Robert Bartha
Robarts Research Institute
Western University
Box 5015, 100 Perth Drive
London, Ontario,
N6A 5K8
CANADA
Tel: 01 519 663 5777 x24039
Fax: 01 519 931 5224
Email: rbartha@robarts.ca

Grant support:
Alzheimer Society of Canada, Ontario Research Fund

Running Title: Brain Ventricle Segmentation

Abstract

Background: A robust algorithm called VAST (Ventricle Analysis combining Shape and Texture segmentation) was developed that combines texture and shape based segmentation to measure the lateral brain ventricle volume from T_1-weighted magnetic resonance imaging (MRI).

New Method: Multiple seeded intensity/texture based fuzzy connectedness and shape based expectation maximization algorithms were uniquely combined with novel automated seed placement.

Results: VAST was validated with a 3D ventricle phantom and its measured volume was within 1% of the known ventricle volume.

Comparison with Existing Methods: A random subset of images was chosen from the Alzheimer's Disease Neuroimaging Initiative (ADNI) database (25 healthy elderly subjects (NEC), 25 people with mild cognitive impairment (MCI) and 25 people with Alzheimer's disease (AD)) acquired at baseline and at 24 months. Ventricle volumes measured with VAST correlated with volumes measured by FreeSurfer and the Boundary Shift Integral (BSI) method, both with R^2 values >0.99. Similarly, ventricle volume changes measured over 24 months by VAST were highly correlated (R^2>0.94) with those measured by FreeSurfer and BSI. Comparing volume changes between groups, all three methods found a significant difference between NEC and people with MCI (p<0.01) as well as between NEC and people with AD

(p<0.01). Only the VAST and BSI algorithms detected significant differences (p<0.05) between people with MCI and AD.

Conclusions: VAST represents a robust novel algorithm for the segmentation of lateral brain ventricles from T_1-weighted MRI. VAST uniquely uses deformable registration to automatically map seed points and combines intensity/texture with shape based segmentation methods to increase accuracy.

Key Words: brain, ventricle, segmentation, MRI, texture, shape

1 Introduction

Alzheimer disease (AD) is the most frequent type of dementia in the elderly affecting an estimated 27-36 million people worldwide (Suzman, 2011) with that number expected to grow significantly in the coming decades in developing countries (Acosta, 2009). Symptoms of this disease include loss of memory and cognitive function decline (Fong et al., 2012; Vellas et al., 2012). However, by the time a diagnosis of AD is made based on memory and functional decline, significant damage has occurred in the brain (Bateman et al., 2012; Fletcher, 2012; Meiner and Rosenmann, 2012). There is growing evidence that neuropathological features develop in persons afflicted with AD well before they develop recognizable symptoms (Braak and Braak, 1991, 1997; Ewers et al., 2011; Hunter et al., 2012; Kao et al., 2012; Mendez et al., 2012; Mori et al., 2012). These pathological changes lead to cell death that can be detected by measurements of tissue atrophy from repeated high resolution magnetic resonance imaging (MRI) (Canu et al., 2011; Gu et al., 2010; Logue et al., 2011; Teipel et al., 2011). Identification of structural changes in the brain during the course of AD could aid diagnosis and predict cognitive deterioration.

To provide a mechanism for the early detection of the onset of AD, several MRI methods have been previously developed to measure changes in the volume of specific brain structures during the course of healthy aging, mild cognitive impairment (MCI), and dementia (Bradley et al., 2002; Fox et al., 2000; Jack et al., 2004; Schott et al., 2005; Wang et al., 2002). Early studies used manual tracings and intensity thresholds to examine volume differences in ventricular and extracerebral cerebrospinal fluid (CSF) spaces (Bradley et al., 2002; Forstl et al., 1995; Murphy et al., 1993; Tanabe et al., 1997), as well as the hippocampal formation (Devanand et al., 2007;

Jack et al., 1997; Jack et al., 2004; Leinsinger et al., 2003; Mu et al., 1999), the amygdala (Cherbuin et al., 2011; Mahanand et al., 2012; Mu et al., 1999; Petersen et al., 2000; Smith et al., 2012) and temporal horn of the lateral ventricles (Bresciani et al., 2005; El Fakhri et al., 2003; Giesel et al., 2006; Hattori et al., 2007; Macdonald et al., 2012; Mu et al., 1999; Thompson et al., 2004). Manual methods remain advantageous in some instances when the anatomical boundaries of structures are difficult to discern and an expert tracer can incorporate knowledge of brain anatomy to identify edges. However manual methods are also highly susceptible to bias and become impractical for clinical use and for the analysis of large datasets.

With the increasing need to efficiently process large numbers of high-resolution images for clinical evaluation or pharmaceutical trials, efforts have focused on developing robust automated image segmentation methods. Some recently developed automated segmentation methods use tissue probability maps based on an atlas or template to measure gray matter, white matter, or whole brain volumes as well as ventricular, hippocampal or amygdala volumes (Keihaninejad et al., 2010; Kovacevic et al., 2009; Ott et al., 2010; Yamashita et al., 2010). Contour level sets have also been employed in automated segmentation methods to identify specific brain regions, white matter, and gray matter (Arimura et al., 2008). Other automated segmentation methods combine landmarks (Giesel et al., 2006) with automated recursive segmentation to measure ventricular, intracranial, or total brain volumes (Carlson et al., 2008; Silbert et al., 2003). Manual and semi-automated segmentation methods require user interaction to make corrections that may lead to bias and slow analysis. Atlas based methods are fully automated allowing non-biased efficient analysis of many images. However, atlas based methods rely on nonlinear registrations and tissue probabilities to map volumes (Fischl et al.,

2002). Inaccuracies in registration can lead to errors in volume measurements (Fonov V S, 2010). Usually minor manual adjustments or corrections are required to refine the automated segmentation (Fischl et al., 2002; Fischl et al., 2004; Han and Fischl, 2007; Segonne et al., 2004). Many studies register multiple atlases and select the atlas that has the smallest registration error to compensate for these inaccuracies, however this approach increases processing time (Jia H et al., 2012). A fully automated method that performs direct segmentation on subject images is not susceptible to registration error.

Some automated segmentation methods are designed to measure volume change between a baseline and a follow-up scan, rather than calculating an absolute volume at a particular time-point. For example the boundary shift integral (BSI) and related techniques can be used to measure whole brain, hippocampal and ventricular atrophy (Ferrarini et al., 2006; Freeborough and Fox, 1997; Jack et al., 2004; Jack et al., 2008; Preboske et al., 2006; Schott et al., 2005; Smith et al., 2007). Measuring volumes at two separate time points and calculating their difference can lead to noisy results, particularly when analyzing small structures. One of the advantages of the BSI method is that it does not measure volumes at two separate time points but measures a differential volume reducing the variability encountered when analyzing a small number of images. The disadvantages of the BSI method include susceptibility to motion, noise, and the presence of non-congruent image contrast (Preboske et al., 2006). The accuracy of atrophy measurements made by segmenting volumes at two separate time points can be increased by accounting for detailed surface features, and decreasing image noise by anisotropic diffusion smoothing and edge enhancement (Ibanez and Schroeder, 2005).

Other semi-automated segmentation methods utilize voxel-based region growing and/or fuzzy methods (Barra et al., 2002; Jack et al., 2005; Nestor et al., 2008). Specifically, Jack *et. al.* (Jack, Shiung et al. 2005) developed automated segmentation software that combines template-based fuzzy clustering, fuzzy inference, and region growing techniques to automatically extract the intracranial cavity, the CSF, and white matter hyperintensities. Barra *et. al.* (Barra et al., 2002) implemented a possibilistic clustering (Krishnapuram and Keller, 1993) fuzzy classification step using wavelet coefficients, resulting in fuzzy map distributions of WM, GM and CSF. Regionally specific volumetric changes of various brain structures including the lateral ventricles have also been studied in the Alzheimer's Disease Neuroimaging Initiative (ADNI) dataset using surface deformation (Qiu et al., 2009). Fuzzy based methods are mathematically precise and provably accurate (Udupa and Saha, 2003). Due to their mathematical exactness, however, time consuming optimization of parameters is necessary. Accurate seed placement is also required in fine structures, which can be difficult to automate. However, fuzzy methods are advantageous because images are directly and accurately processed and such methods are not prone to misclassification due to registration errors.

In studies examining the changes in brain structure in Alzheimer disease, ventricular enlargement is commonly shown to be a robust metric for assessing disease progression (Apostolova et al., 2012; Chetelat and Baron, 2003; Chou et al., 2009). Using a variety of segmentation techniques to measure ventricle volumes, it is possible to distinguish between groups of elderly healthy patients, subjects with MCI and subjects with AD (Nestor et al., 2008), to detect progression of MCI subjects to AD (Jack et al., 2008; Whitwell et al., 2008), or to associate changes in ventricle volume with decreasing levels of amyloid-beta peptide (Aβ) in

CSF (Ott et al., 2010). For example, a recursive automated method to measure ventricular, intracranial, and total brain volumes (Carlson, Moore et al. 2008) was developed by successively applying a discriminant function to the established tissue type sample intensities and "peeling" away or isolating regions (bone, brain, CSF, etc.) of the image. Annual rates of ventricular expansion were greater in subjects who developed MCI in follow-up than those that were cognitively stable (Carlson, Moore et al. 2008). Specifically, ventricular volume expansion was found ~2.3 years prior to a clinical diagnosis of MCI. Voxel-based morphometry (VBM) with Statistical Parametric Mapping 5 (SPM 5) has also shown widening of the lateral ventricles and Sylvian fissures in patients with idiopathic normal pressure hydrocephalus (iNPH), compared to AD patients and healthy controls (Yamashita et al., 2010). Thus ventricle volume expansion features have proven to be excellent biomarkers for studying AD, particularly for early detection. Measurement of ventricular change can significantly reduce the number of subjects required to detect a treatment effect in clinical trials (Nestor et al., 2008). Despite the success of brain ventricle measurements in the past, most algorithms have difficulty in accurately segmenting the fine details of the temporal horns.

Due to the emerging importance of brain ventricle quantification in Alzheimer disease and other neurological disorders, the purpose of this work was to develop a novel brain structure segmentation procedure that combined the best attributes of previous methods and merged intensity and shape based approaches, to improve the accuracy and precision of brain ventricle segmentation. Such an algorithm could increase the efficiency of the evaluation of new drugs in clinical trials, and impact clinical patient management. We propose an automated brain ventricle segmentation algorithm called VAST (Ventricle Analysis combining Shape and Texture

segmentation) that combines template-based deformable registration to automatically place landmarks (seeds), an accurate fuzzy connectedness segmentation that uses these seeds, and a probability map based Expectation-Maximization (EM) segmentation to extract fine details. Manual cropping is used to remove unwanted structures, followed by correction for tissue partial volume. This algorithm was initially designed to measure the lateral brain ventricle volume from T_1-weighted MRI images because there is a high contrast between the cerebral spinal fluid within the ventricle and the surrounding tissue, however it could be extended to other structures in the future. The method was validated using a physical brain ventricle phantom and tested on a random subset of data from the Alzheimer's Disease Neuroimaging Initiative (ADNI) to compare to existing segmentation methods, namely FreeSurfer and BSI.

2 Methods

2.1 Algorithm

The VAST algorithm to quantify brain ventricle volume is summarized in Figure 1 and was designed to optimize accuracy and reproducibility while maintaining automation. Existing registration and segmentation methods were adapted and combined in the Insight Segmentation and Registration Toolkit (ITK) (Ibanez and Schroeder, 2005; Yoo et al., 2002) and 3D Slicer3 (Fedorov et al., 2012; Gering et al., 1999; Pieper et al., 2004; Pieper et al., 2006). The algorithm involves the following steps:

1. Definition of Seed Points in Atlas: A single series of brain image slices was chosen as an atlas or template and predefined seeds were selected within the lateral and third ventricles. Seed points were automatically mapped from 10 seeds in each of the left and right main body, posterior horns, and temporal horns of ventricles within the atlas to the corresponding regions in the ventricles in each subject, resulting in a total of 60 mapped

seeds. This mapping utilized a deformation field obtained from a multi-scaled diffeomorphic deformable registration (Vercauteren et al., 2007a; Vercauteren et al., 2007b) that warps the brain of the subject into the atlas. For computational efficiency, the subject was first affinely registered (Ibanez and Schroeder, 2005) to the atlas prior to warping. To improve the accuracy of the seed mapping, the warping was restricted to a region surrounding the contour of the ventricles in the atlas by masking. Histogram matching (Gonzalez and Woods, 1992; Ibanez and Schroeder, 2005; Lim, 1990) was used to further improve the accuracy. The choice of the atlas image is arbitrary since its only purpose is to transfer seed points but the modality of the atlas and subject image must be similar. This process of initializing seed points in the subject images was performed in parallel using the original subject images as well as the subject images following gradient anisotropic diffusion filtering (Ibanez and Schroeder, 2005; Perona and Malik, 1990; Ter Romeney, 1994) for smoothing image noise and enhancing image edges.

2. Confidence Connected Segmentation: The mean and standard deviation of the image intensity of the mapped seed points were used to generate a rough segmentation using a confidence connected algorithm (Ibanez and Schroeder, 2005). Pixels within three standard deviations of the mean were included in the initial segmentation. However, the variance multiplier was adjusted using a binary search algorithm on subsequent iterations to achieve the most complete segmentation. Separate segmentations were performed for six different regions of the ventricle (the left and right body, the left and right posterior horns, and the left and right temporal horn regions). The segmented result from each region was combined into one final result. Using multiple regions allowed the optimization of the variance multiplier for each region.

3. Fuzzy Connected Segmentation: The mean and standard deviation of all voxels for a region included in the confidence connected segmentation were used to initialize a fuzzy connectedness algorithm (Saha and Udupa, 2001). Fuzzy connectedness is based on strengths measured by a fuzzy affinity function. A Gaussian fuzzy affinity function was used as described in (Udupa and Samarasekera, 1995) that scales the contributions from the image intensities and the gradients of the voxels. By combining both intensity and gradient information, the affinity calculation is expected to be more robust with respect to noise (Jones and Metaxas, 1997). Fuzzy connectedness calculates strengths of paths between voxels. The strength of a path is defined as the smallest fuzzy affinity value or weakest link between any two voxels along a particular path. This strength indicates how well voxels are connected: hence the term fuzzy connectedness. In the fuzzy connectedness algorithm, the strengths of all possible paths from the seeds to the voxels are calculated, the strongest path is chosen and a map or scene of fuzzy affinity-based connectedness values is generated based on these strengths. Then using a threshold value ranging between 0 and 1, voxels from the scene that have an affinity value above this threshold are included in the segmented ventricle volume and those below the threshold are excluded. A threshold value of 0.5 was used in the current study. To reduce processing time, we incorporated multiple seeds with the fuzzy connectedness algorithm, and implemented an efficient *kθFOEMS* algorithm (*kθ-fuzzy object extraction for multiple seeds)* described in (Saha and Udupa, 2001). Once the algorithm finds a path of strength between a voxel and a particular seed that is greater than the strength of any other path between another voxel to that seed, it does not need to search for a better path. Using multiple seeds effectively fills the affinity scene sooner, reducing computation

time. Ventricles were segmented using fuzzy connectedness in both anisotropic diffusion smooth filtered and original, unfiltered images and the results were merged (Figure 1). The segmentation of the smooth filtered images improved performance under conditions of low signal to noise ratio.

4. Shape Based Segmentation: To accurately capture the fine surface details surrounding the main body of the ventricles an automated shape-based Expectation Maximization (EM) segmentation method (Pohl et al., 2007) included with the Slicer3 software was used to segment each image into component grey matter (GM), white matter (WM), and the cerebrospinal fluid (CSF). The EM algorithm (Dempster et al., 1977; McLachlan and Krishnan, 1997) is used in Slicer3 in a Bayesian statistical model to determine optimal parameters for an automated joint registration and segmentation algorithm that relies on prior information to segment brain structures. It uses registration and segmentation in a complementary way. By accurately modeling image artifacts (such as image inhomogeneity or a subject-specific intensity histogram of an anatomical structure) and accurately registering shape prior information using an atlas (such as knowing that the ventricles are above the thalamus), it uses deformable registrations of subjects with an atlas to successfully segment structures with weakly visible boundaries. For example, aligning the atlas with the subject helps detect the thalamus. Once the thalamus is segmented, this in turn simplifies the registration of weakly visible boundaries between the thalamus and white matter. In mathematical terms, the EM algorithm (Dempster et al., 1977; McLachlan and Krishnan, 1997) iterates between an E-step and an M-step. In the E-step, it creates a function for the expectation of the log-likelihood of the artifacts (called nuisance parameters) and registration parameters using a current estimate of these

parameters. In the M-step, it computes parameters maximizing the expected log-likelihood found in the E-step. These parameters are then used on the next E-step to calculate an updated expectation log-likelihood function, and the process is repeated until the global maximum expected log-likelihood of the nuisance and registration parameters are reached. It also organizes the registration parameters in a hierarchy from global registration parameters that apply to the entire atlas and image down to structure-dependent registration parameters for local deformations within anatomical regions (Pohl et al., 2006).

5. Merge Shape Based Segmentation with Fuzzy Segmentation: The whole brain CSF portion of EM label map was automatically merged with the fuzzy connected segmentation of the entire ventricle (including the body and horns) using ITK's MergeLabelMapFilter class. Merging was necessary because in noisy subjects, the EM label map had pitted holes in the ventricle body, but merging the fuzzy connected segmentations of the smoothed and original image resulted in a smooth segmentation of the ventricle body, even when the images were noisy. The EM label map, on the other hand, consistently captured the thin temporal horn regions, including isolated pieces of the horns when the 1.2 mm^3 pixel resolution of the image was not able to resolve thin connections. This step compensated for instances when seeds were not mapped into the isolated regions of the thin temporal horns, resulting in these regions being missed by the fuzzy connected segmentation. Thus combining both methods resulted in more robust segmentations. These isolated pieces were added using the Slicer3 Save Islands feature (Fedorov et al., 2012; Gering et al., 1999; Pieper et al., 2004; Pieper et al., 2006).

6. Cropping: Segmentations were cropped manually to remove the third ventricle using the Slicer3 Editor Module.
7. Partial Volume Error Corrections: A random Markov field process was used to classify mixed tissue voxels (Tohka et al., 2004), based on the gray matter, white matter and CSF Expectation Maximization segmentation (Pohl et al., 2006). In a fully automated manner, the cropped fuzzy segmentation was dilated and overlaid with the mixed tissue classification (Figure 2) to refine the volume calculation. A linear interpolation model based on the intensities of voxels surrounding the mixed tissue was used to estimate the CSF fraction of mixed pixels.

2.2 Algorithm Validation

The VAST algorithm was first tested using images of a brain ventricle phantom designed for validation of ventricle segmentation methods from T_1-weighted MRI (Khan et al., 2012). The brain ventricle phantom images were acquired using a T_1-weighted anatomical imaging sequence at 3T: ADNI-specific 3D magnetization prepared rapid gradient-echo (MP-RAGE) sequence (2300/2.98 [TR/TE]; matrix, 256 x 240; flip angle, 9; field of view, 256 mm). Images of the phantom were acquired with an in-plane resolution of 1.0 mm^2, with slice thicknesses of 1.0 mm (Khan et al., 2012).

To determine whether the algorithm was sensitive to changes in ventricle volume over time in human subjects, images from the Alzheimer's Disease Neuroimaging Initiative (ADNI) database (adni.loni.ucla.edu) were used to measure ventricle expansion in normal elderly controls (NEC),

people with mild cognitive impairment (MCI), and people with diagnosed Alzheimer's disease (AD).

Data used in the preparation of this article were obtained from the Alzheimer's Disease Neuroimaging Initiative (ADNI) database (adni.loni.ucla.edu). The ADNI was launched in 2003 by the National Institute on Aging (NIA), the National Institute of Biomedical Imaging and Bioengineering (NIBIB), the Food and Drug Administration (FDA), private pharmaceutical companies and non-profit organizations, as a $60 million, 5-year public-private partnership. The primary goal of ADNI has been to test whether serial magnetic resonance imaging (MRI), positron emission tomography (PET), other biological markers, and clinical and neuropsychological assessment can be combined to measure the progression of mild cognitive impairment (MCI) and early Alzheimer's disease (AD). Determination of sensitive and specific markers of very early AD progression is intended to aid researchers and clinicians to develop new treatments and monitor their effectiveness, as well as lessen the time and cost of clinical trials.

The Principal Investigator of this initiative is Michael W. Weiner, MD, VA Medical Center and University of California – San Francisco. ADNI is the result of efforts of many co-investigators from a broad range of academic institutions and private corporations, and subjects have been recruited from over 50 sites across the U.S. and Canada. The initial goal of ADNI was to recruit 800 subjects but ADNI has been followed by ADNI-GO and ADNI-2. To date these three protocols have recruited over 1500 adults, ages 55 to 90, to participate in the research, consisting of cognitively normal older individuals, people with early or late MCI, and people with early

AD. The follow up duration of each group is specified in the protocols for ADNI-1, ADNI-2 and ADNI-GO. Subjects originally recruited for ADNI-1 and ADNI-GO had the option to be followed in ADNI-2. For up-to-date information, see www.adni-info.org.

Baseline and 24-month follow-up T_1-weighted images were obtained from twenty-five subjects randomly selected from each group (demographic information is presented in Table 1). Ventricle volumes were measured using the algorithm described above. Ventricle volume changes over 24 months were compared with available ventricle volume changes measured by FreeSurfer and the BSI method that were downloaded directly from the ADNI web site. For each method, paired t-tests were used to determine whether the ventricle volume changed significantly over the two year period. Group comparisons were also made using unpaired t-tests to determine whether the change in ventricle volume was different between groups. In all cases, $p<0.05$ was considered statistically significant.

These data were also used to assess several features of the algorithm. First, the benefit of combining fuzzy segmentation with EM segmentation was evaluated by segmenting the ventricle using fuzzy segmentation alone and in combination with EM segmentation. The measured ventricle volume at baseline was compared using both approaches as well as the measured change over 24 months. Second, the reliability of the manual cropping of volume outside the lateral ventricles (algorithm step six) was tested by comparing final ventricle volumes after cropping between four different raters working independently on the same images. Each rater was trained by an expert experienced in using 3D Slicer and incorporated knowledge of the ventricle anatomy. Each rater cropped the set of 25 baseline images and 25 images at 24 months

from each of the NEC, MCI and AD groups. The cropped images were examined by the expert. Raters were non-experts in image segmentation or brain anatomy. Intra-class correlation coefficients were calculated using cropped volumes from three raters on the 25 AD baseline images.

3 Results

The measured volume of the ventricles in the 3D ventricle phantom was 47.2 cm^3 as previously reported (Khan et al., 2012) This value is less than 1% different than the specific gravity derived volume of 47.67 cm^3 and less than 0.1% larger than overflow can measurement volume of 47.16 cm^3 (Khan et al., 2012). Figure 2 shows the result of a typical ventricle segmentation in a subject with Alzheimer's disease. The very thin portions of the temporal horn are accurately segmented by VAST. Baseline ventricle volumes measured with VAST correlated well with volumes measured by FreeSurfer (Figure 3A) and the BSI method (Figure 3B), both with R^2 values >0.99. The correlation of VAST volumes with FreeSurfer and BSI volumes produced slopes slightly less than 1 (0.9499 for FreeSurfer and 0.9821 for BSI), and small intercepts (2.02 for FreeSurfer and 3.30 cm^3 for BSI). These slopes and intercepts suggest that on average, the ventricle volumes obtained by the VAST method were slightly larger than the volumes obtained by the BSI method or FreeSurfer. The change in ventricle volume after 24 months is provided in Figure 4 for VAST, FreeSurfer, and the BSI method. All three methods showed similar significant increases (Table 2) in ventricle volume (~3.6 cm^3 in healthy elderly,~8.0 cm^3 in people with mild cognitive impairment, and ~11.7 cm^3 in people with Alzheimer's disease, Figure 4).

Comparing volume changes within groups (Table 2), all three methods found significant differences (p<0.01) over 24 months in normal elderly, people with MCI, and people with AD. Comparing volume changes between group, differences were detected by all three methods (p<0.01) when comparing normal elderly to people with AD, and comparing normal elderly to people with MCI. However, a group difference between people with MCI and people with AD was more difficult to detect. The VAST and BSI algorithms detected differences (p<0.05, Table 2) while the FreeSurfer method did not (p=0.15). The measured ventricle volume changes measured by VAST were highly correlated (R^2>0.94) with those measured by FreeSurfer (Figure 5A) and BSI (Figure 5B). In each case, there was a small positive y-intercept indicating at small ventricle volumes, FreeSurfer and the BSI measured larger volumes, however, this trend was reversed for large ventricle volumes producing a slope that was less than one (0.87-0.89).

Comparison of measured ventricle volume and volume changes over 24 months when using Fuzzy segmentation (algorithm step three) and Fuzzy merged with shape-based EM segmentation (algorithm steps four and five) are shown in Figures 6A and 6B. Using a paired t-test to compare ventricle volume change over 24 months using Fuzzy segmentation alone compared to using Fuzzy segmentation combined with EM segmentation, showed significance (p<0.01) only within the MCI group. For the NEC and AD groups, p>0.3. The increase in volume is attributed to better segmentation of the temporal horns in cases when a thin horn is difficult to isolate (Figure 7).

The only step in the algorithm that required manual intervention was step six – the manual cropping of CSF extraneous to the lateral ventricle. However, intra class correlation was 1.0,

indicating excellent agreement and consistency. A Bland-Altman plot including results for all raters (Figure 8) indicates no bias as a function of ventricle volume and shows the maximum difference between two raters was ~0.6 cm^3.

4 Discussion

A new protocol was successfully developed and tested for segmentation of the lateral ventricles in the brain from T_1-weighted magnetic resonance images. The algorithm accurately segmented the ventricles in a brain ventricle phantom, and was able to detect group differences between subjects aging normally and subjects with mild cognitive impairment or with Alzheimer's disease using only twenty-five image sets per group. A significant increase in ventricle volume was detected in all groups after two years. This volume change was significantly different between all three subject groups.

There are several features of the algorithm that are unique and that enable highly reproducible measurement. Because the VAST algorithm directly segments the acquired images, it is not prone to registration errors as are registration-based segmentation methods and thus does not require manual corrections. It also allows image noise reduction and edge enhancement because the algorithm works directly on the acquired images. Also, the VAST method is the first to use deformable registration to automatically map seed points from an atlas to each subject image. This step eliminated the need for manual seed placement and allowed a large number of seeds to be placed in each image. A large number of seeds enables the optimization of the local mean and variance of the pixel intensities for the fuzzy segmentation independently within different regions (left body, right body, left temporal horn, right temporal horn, left posterior horn, right

posterior horn). Second, combining intensity/texture based methods that work well on the ventricle body with shape based methods which work well on the horns has produced an accurate and robust lateral ventricle segmentation. The EM label map was able to consistently capture the thin temporal horn regions, including the isolated pieces of the horns when the 1.2 mm^3 pixel resolution of the image was not able to resolve thin connections. This feature compensated for instances when seeds were not mapped into the isolated regions of the thin temporal horns, resulting in these regions being missed by the fuzzy connected segmentation. Thus, without EM segmentation, the temporal horns are less accurate and group differences are not as reliably detected. However, in images with low signal to noise ratio, the EM label map had pitted holes in the ventricle body. Therefore, merging the fuzzy connected segmentation of the smoothed and original image resulted in a smooth segmentation of the ventricle body, even when the images were noisy.

The ventricle volumes measured by VAST, FreeSurfer, and BSI were comparable. Tissue partial volume correction was required for the VAST measured volumes to be consistent with previous methods (FreeSurfer and the BSI method). Without partial volume corrections, the measured volumes from the VAST algorithm were consistently underestimated. The VAST volumes tended to be slightly larger than the other methods when large ventricles were measured, and smaller when small ventricles were measured. This result is consistent with previous studies that have shown that FreeSurfer may overestimate hippocampal volume measurements (Nestor et al., 2012; Sanchez-Benavides et al., 2010; Wang et al., 2011). The only step in the VAST method that required manual intervention was the cropping of CSF outside the lateral ventricles. This CSF was often observed in the third and fourth ventricles as well as in sulci, particularly in

cases of severe atrophy as are typically observed in the patients with Alzheimer's disease. However, results were highly reproducible between raters when including manual cropping (Figure 8).

The VAST results were strongly correlated with results using both FreeSurfer and BSI. However there are significant differences between the algorithms. FreeSurfer is a registration based segmentation while VAST operates directly on the acquired images, making VAST less prone to registration errors. VAST also takes half the processing time required by FreeSurfer. VAST does not require both a baseline and follow-up image to calculate a ventricle volume, which is required by BSI. Also, like BSI, VAST was able to detect significant changes ($p<0.05$) between all three groups when comparing volumes and volume change, while FreeSurfer was not able to detect a significant difference between AD and MCI ($p=0.15$) when comparing volume change (Table 2). The change in ventricle volume over two years measured by VAST based on all 25 subjects from each group (NEC, MCI and AD), were 3.2 cm^3 for elderly controls, 7.5 cm^3 for people with MCI, and 11.5 cm^3 for people with AD. These changes are consistent with a previous report of annual ventricle expansion of 1.7 cm^3/year for 40 stable elderly controls, 2.6 cm^3/year for 15 stable people with MCI, and 6.4 cm^3/year for 33 people with fast progressing AD (Jack et al., 2004).

In the future, an automated cropping algorithm will be developed that will make the algorithm fully automated allowing the processing of a large number of images in a seamless and time efficient manner. In addition, the deformable registration will be used to identify sub-regions of

the ventricles to isolate differences in ventricle expansion in the temporal horns and anterior portions of the lateral ventricle.

In summary, a robust algorithm has been described for segmenting the lateral brain ventricles using MRI. VAST uniquely uses deformable registration to automatically map seed points and directly segment the ventricles in acquired images. The algorithm was validated using a ventricle phantom with known volume and showed excellent agreement with well-known methods such as FreeSurfer and BSI. The sensitivity to detect group differences in ventricle expansion was as good or better than FreeSurfer and BSI.

Acknowledgements

The authors thank James Im, Cecilia Kwok, Elena Mamycheva and Jack Li for performing repeated trials of manual cropping, and Alex Hayes for performing the manual croppings to compare Fuzzy segmentation alone to Fuzzy + EM segmentation. Funding was provided by a two year Post-Doctoral Fellowship from the Alzheimer Society of Canada and a Research Grant from the Ontario Research Fund (ORF).

Data collection and sharing for this project was funded by the Alzheimer's Disease Neuroimaging Initiative (ADNI) (National Institutes of Health Grant U01 AG024904). ADNI is funded by the National Institute on Aging, the National Institute of Biomedical Imaging and Bioengineering, and through generous contributions from the following: Alzheimer's Association; Alzheimer's Drug Discovery Foundation; BioClinica, Inc,; Biogen Idec Inc.; Bristol-Myers Squibb Company; Eisai Inc.; Elan Pharmaceuticals, Inc.; Eli Lilly and Company;

F. Hoffmann-La Roche Ltd and its affiliated company Genentech, Inc.; GE Healthcare; Innogenetics, N.V.; IXICO Ltd.; Janssen Alzheimer Immunotherapy Research & Development, LLC.; Johnson & Johnson Pharmaceutical Research & Development LLC.; Medpace, Inc.; Merck & Co., Inc.; Meso Scale Diagnostics, LLC.; NeuroRx Research; Novartis Pharmaceuticals Corporation; Pfizer Inc.; Piramal Imaging; Servier; Synarc Inc.; and Takeda Pharmaceutical Company. The Canadian Institutes of Health Research is providing funds to support ADNI clinical sites in Canada. Private sector contributions are facilitated by the Foundation for the National Institutes of Health (www.fnih.org). The grantee organization is the Northern California Institute for Research and Education, and the study is coordinated by the Alzheimer's Disease Cooperative Study at the University of California, San Diego. ADNI data are disseminated by the Laboratory for Neuro Imaging at the University of California, Los Angeles. This research was also supported by NIH grants P30 AG010129 and K01 AG030514.

Conflicts of Interest

John Drozd: None.
Robert Moreland: None.
Samaneh Kazemifar: None.
Michael Borrie: None.
Robert Bartha is the Chief Scientific Officer and a shareholder of Bioscape Imaging Solutions Inc.

Contributions

John Drozd: contributed to software conceptualization, wrote all software, completed all experiments, analyzed the data, and wrote the manuscript.
Robert Moreland: contributed to software conceptualization and writing, and critically reviewed the manuscript
Samaneh Kazemifar: contributed to software conceptualization and writing, and critically reviewed the manuscript
Michael Borrie: contributed to study conceptualization and critically reviewed the manuscript
Robert Bartha: conceived the study, contributed to software conceptualization, designed the study, interpreted results, and wrote the manuscript.

All authors have approved the final article for submission.

Figures

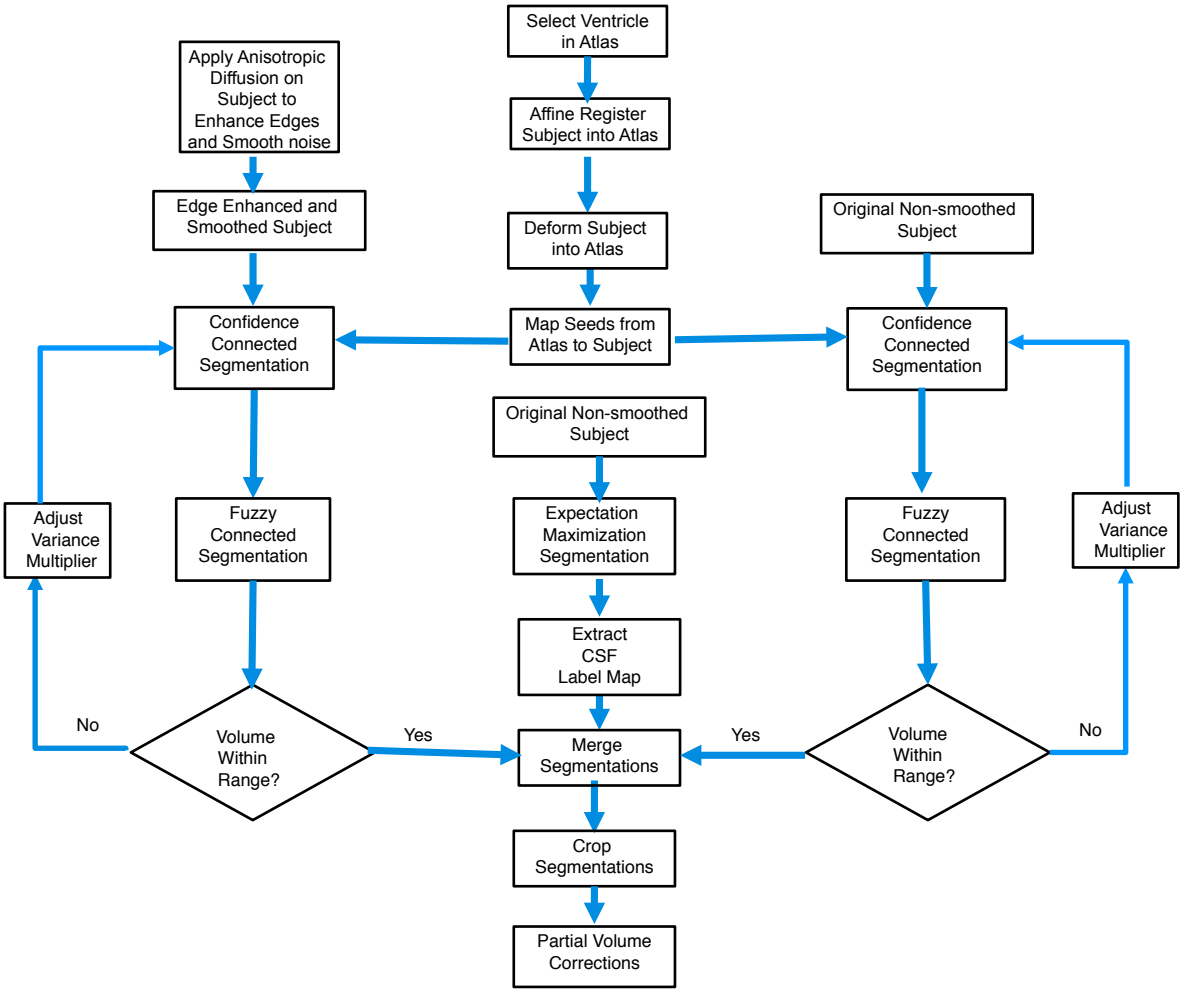

Figure 1: Flow chart of brain ventricle segmentation algorithm.

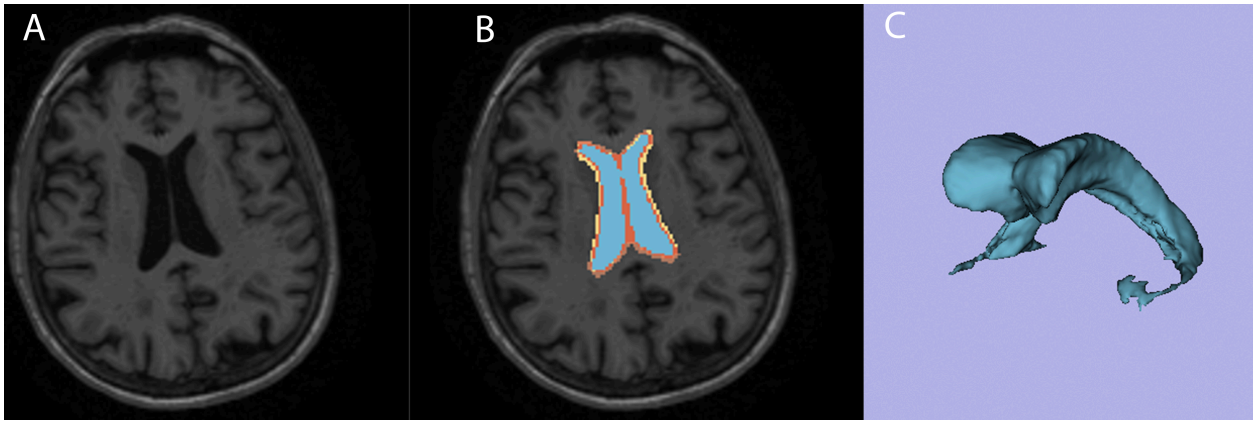

Figure 2: Axial T_1-weighted MRI of a subject with AD (A). Lateral ventricle CSF pixels highlighted in blue and mixed tissue voxels as brown and yellow pixels (B). A three-dimensional representation of the ventricle from this subject (C) demonstrates the thin temporal horn details that are detected.

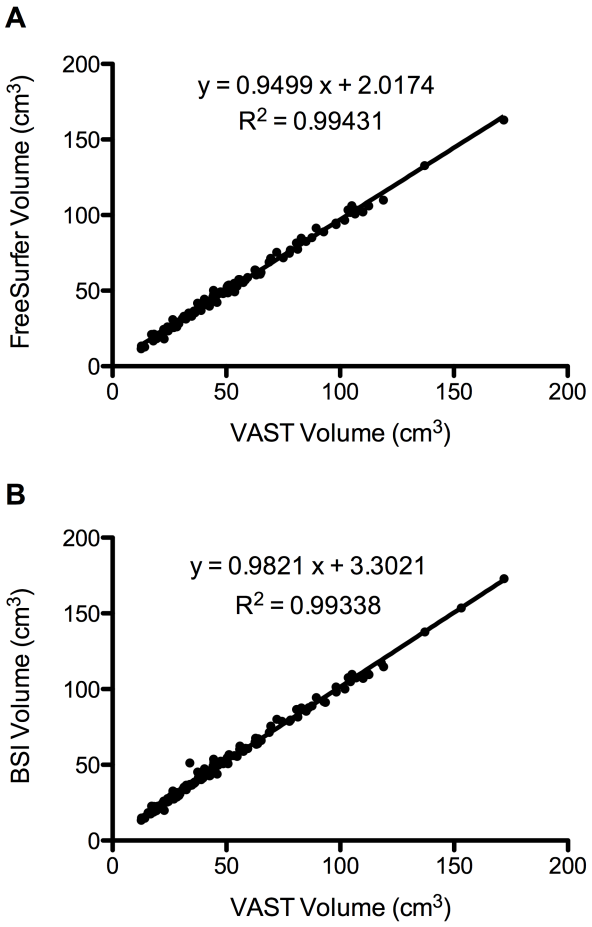

Figure 3: Partial volume corrected ventricle volumes measured by VAST compared to volumes measured by FreeSurfer (A) and BSI (B). Analysis included only randomly selected subjects that had volumes reported on the ADNI website using FreeSurfer and BSI. This analysis included 20 NEC baseline and 23 NEC followup subjects, 16 MCI baseline and 24 MCI followup subjects, and 20 AD baseline and 25 AD followup subjects for comparisons with FreeSurfer (A), and 25 NEC baseline and 23 NEC followup subjects, 25 MCI baseline and 21 MCI followup subjects and 25 AD baseline and 23 AD followup subjects for comparisons with BSI (B).

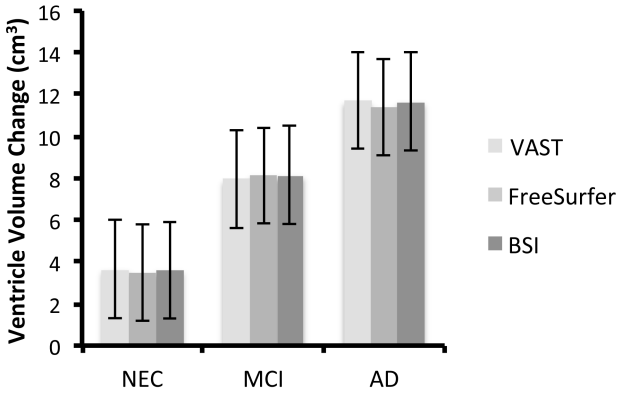

Figure 4: Ventricle volume change over 24 months comparing segmentation methods. Error bars represent standard error of the mean (SEM). The ADNI website did not post FreeSurfer and BSI anatomical volumes of all of the randomly chosen subjects used for this study. Direct comparisons were made with subjects that had volumes reported on the ADNI website from both FreeSurfer and BSI. This analysis included 19 NEC subjects, 12 MCI subjects and 18 AD subjects.

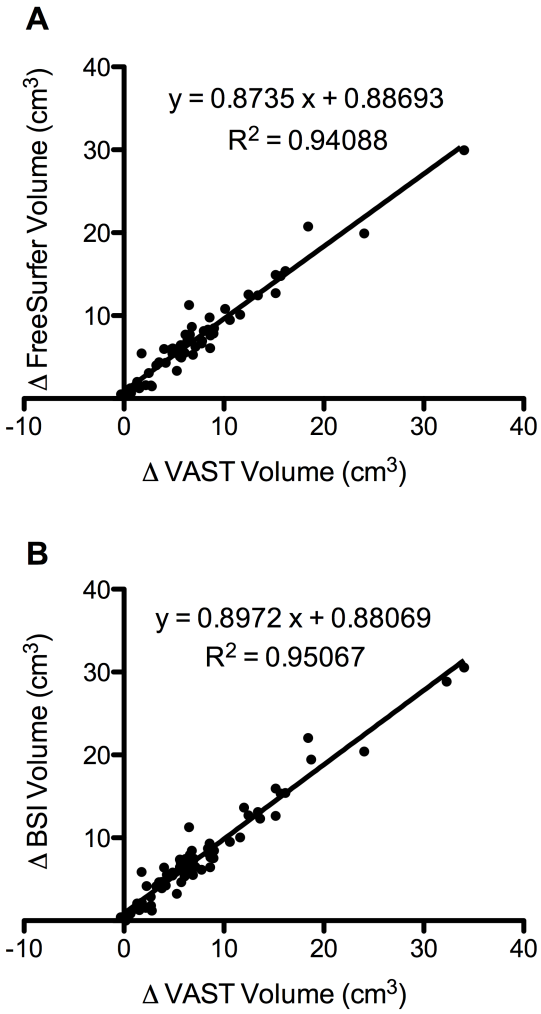

Figure 5: Change in ventricle volume between baseline and 24 months in all subjects measured by VAST compared to FreeSurfer (A) and BSI (B). The ADNI website did not post FreeSurfer and BSI anatomical volumes of all of the randomly chosen subjects used for this study. Correlations included only subjects that had corresponding baseline and followup volumes reported on the ADNI website from FreeSurfer and BSI. This analysis included 20 NEC subjects, 15 MCI subjects, and 20 AD subjects for comparisons with FreeSurfer (A), and 23 NEC subjects, 21 MCI subjects and 23 AD subjects for comparisons with BSI (B).

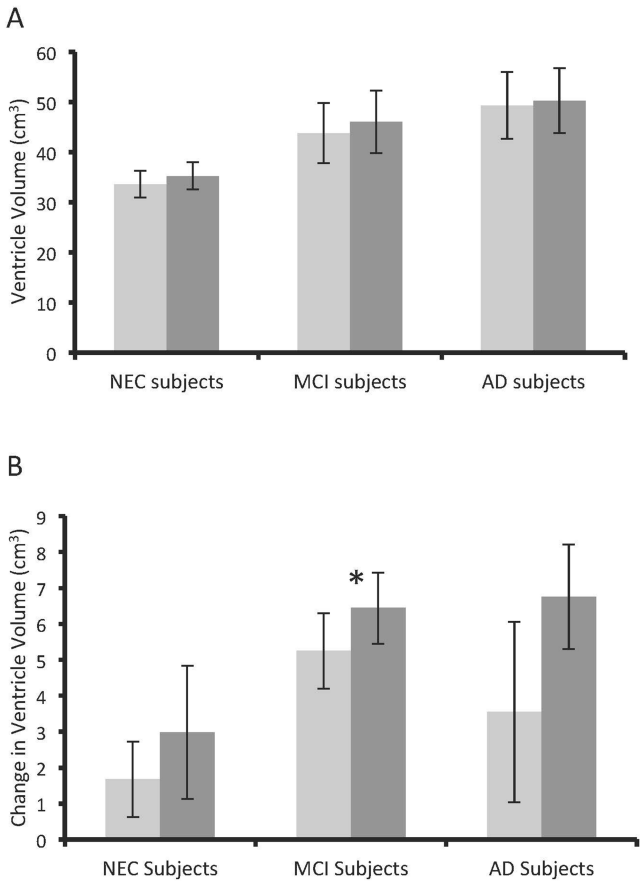

Figure 6: Average baseline ventricle volume using Fuzzy segmentation only (light grey bar) and Fuzzy + EM segmenation (dark grey bar) (A). Change in ventricle volume over 24 months using Fuzzy segmentation only (striped grey bars) and Fuzzy + EM segmentation (solid grey bars) (B). Partial volume corrections are not incorporated. Error bars represent standard error of the mean (SEM). This analysis included 25 NEC subjects, 19 MCI subjects, and 25 AD subjects.

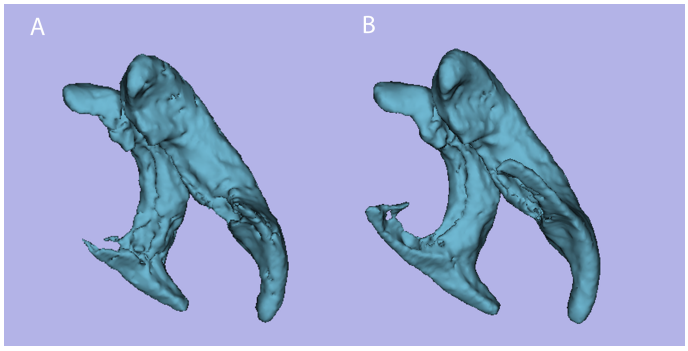

Figure 7: 3D representation of a segmented ventricle from a subject with AD at baseline using Fuzzy segmentation alone (A) and combined Fuzzy + EM segmentation (B). Note the more complete temporal horn segmentation with the combined Fuzzy + EM segmentation.

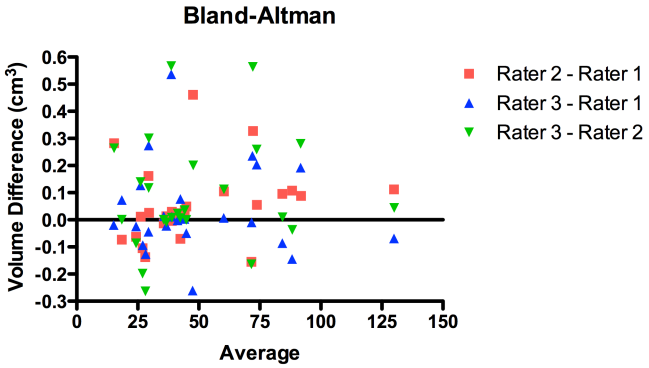

Figure 8: Inter-rater reliability compared for three raters using set of 25 baseline images from the AD group

Tables

Table 1: Subject demographics of 3 groups from ADNI data set.

	NEC	MCI	AD
Population	25	25	25
Age ± (SD) (Baseline)	75.5 (4.7)	74.4 (7.4)	77.3 (6.1)
Sex (M)	15	15	13
ΔMMSE ± (SD)	0 (1.4)	1.8 (2.8)	3.4 (5.6)

Table 2: P values comparing 3 groups from ADNI data set. $P<0.05$ indicates significance.

	VAST	FreeSurfer	BSI
P values Paired t –Test: Comparing Volumes			
NEC at baseline vs. NEC at 24 months	< 0.01	< 0.01	< 0.01
MCI at baseline vs. MCI at 24 months	< 0.01	< 0.01	< 0.01
AD at baseline vs. AD at 24 months	< 0.01	< 0.01	< 0.01
P values Unpaired t-Test: Comparing Volume change			
AD vs. MCI	< 0.05	0.15	< 0.05
NEC vs. MCI	< 0.01	< 0.01	< 0.01
NEC vs. AD	< 0.01	< 0.01	< 0.01

References

Acosta, D., Wortmann, M., 2009. World Alzheimer Report - Executive Summary. In: Prince, M., Jackson J. (Ed.), pp. 6-8.

Apostolova, L.G., Green, A.E., Babakchanian, S., Hwang, K.S., Chou, Y.F., Toga, A.W., Thompson, P.M., 2012. Hippocampal atrophy and ventricular enlargement in normal aging, mild cognitive impairment (MCI), and Alzheimer Disease. Alzheimer Dis Assoc Disord 26(1), 17-27.

Arimura, H., Yoshiura, T., Kumazawa, S., Tanaka, K., Koga, H., Mihara, F., Honda, H., Sakai, S., Toyofuku, F., Higashida, Y., 2008. Automated method for identification of patients with Alzheimer's disease based on three-dimensional MR images. Acad Radiol 15, 274-284.

Barra, V., Frenoux, E., Boire, J.Y., 2002. Automatic volumetric measurement of lateral ventricles on magnetic resonance images with correction of partial volume effects. Journal of Magnetic Resonance Imaging 15, 16-22.

Bateman, R.J., Xiong, C., Benzinger, T.L., Fagan, A.M., Goate, A., Fox, N.C., Marcus, D.S., Cairns, N.J., Xie, X., Blazey, T.M., Holtzman, D.M., Santacruz, A., Buckles, V., Oliver, A., Moulder, K., Aisen, P.S., Ghetti, B., Klunk, W.E., McDade, E., Martins, R.N., Masters, C.L., Mayeux, R., Ringman, J.M., Rossor, M.N., Schofield, P.R., Sperling, R.A., Salloway, S., Morris, J.C., 2012. Clinical and Biomarker Changes in Dominantly Inherited Alzheimer's Disease. N Engl J Med.

Braak, H., Braak, E., 1991. Neuropathological stageing of Alzheimer-related changes. Acta Neuropathol 82, 239-259.

Braak, H., Braak, E., 1997. Staging of Alzheimer-related cortical destruction. Int Psychogeriatr 9 Suppl 1, 257-261; discussion 269-272.

Bradley, K.M., Bydder, G.M., Budge, M.M., Hajnal, J.V., White, S.J., Ripley, B.D., Smith, A.D., 2002. Serial brain MRI at 3-6 month intervals as a surrogate marker for Alzheimer's disease. British Journal of Radiology 75, 506-513.

Bresciani, L., Rossi, R., Testa, C., Geroldi, C., Galluzzi, S., Laakso, M.P., Beltramello, A., Soininen, H., Frisoni, G.B., 2005. Visual assessment of medial temporal atrophy on MR films in Alzheimer's disease: comparison with volumetry. Aging Clin Exp Res 17, 8-13.

Canu, E., McLaren, D.G., Fitzgerald, M.E., Bendlin, B.B., Zoccatelli, G., Alessandrini, F., Pizzini, F.B., Ricciardi, G.K., Beltramello, A., Johnson, S.C., Frisoni, G.B., 2011. Mapping the structural brain changes in Alzheimer's disease: the independent contribution of two imaging modalities. Journal of Alzheimers Disease 26.

Carlson, N.E., Moore, M.M., Dame, A., Howieson, D., Silbert, L.C., Quinn, J.F., Kaye, J.A., 2008. Trajectories of brain loss in aging and the development of cognitive impairment. Neurology 70, 828-833.

Cherbuin, N., Sachdev, P.S., Anstey, K.J., 2011. Mixed handedness is associated with greater age-related decline in volumes of the hippocampus and amygdala: the PATH through life study. Brain Behav 1, 125-134.

Chetelat, G., Baron, J.C., 2003. Early diagnosis of Alzheimer's disease: contribution of structural neuroimaging. Neuroimage 18, 525-541.

Chou, Y.Y., Lepore, N., Avedissian, C., Madsen, S.K., Parikshak, N., Hua, X., Shaw, L.M., Trojanowski, J.Q., Weiner, M.W., Toga, A.W., Thompson, P.M., 2009. Mapping correlations between ventricular expansion and CSF amyloid and tau biomarkers in 240 subjects with Alzheimer's disease, mild cognitive impairment and elderly controls. Neuroimage 46(2), 394-410.

Dempster, A., Laird, N., Rubin, D., 1977. Maximal likelihood from incomplete data via the EM algorithm. Proceedings of the Royal Statistical Society 39, 1-38.

Devanand, D.P., Pradhaban, G., Liu, X., Khandji, A., De Santi, S., Segal, S., Rusinek, H., Pelton, G.H., Honig, L.S., Mayeux, R., Stern, Y., Tabert, M.H., de Leon, M.J., 2007. Hippocampal and entorhinal atrophy in mild cognitive impairment: prediction of Alzheimer disease. Neurology 68, 828-836.

El Fakhri, G., Kijewski, M.F., Johnson, K.A., Syrkin, G., Killiany, R.J., Becker, J.A., Zimmerman, R.E., Albert, M.S., 2003. MRI-guided SPECT perfusion measures and volumetric MRI in prodromal Alzheimer disease. Arch Neurol 60, 1066-1072.

Ewers, M., Frisoni, G.B., Teipel, S.J., Grinberg, L.T., Amaro, E., Jr., Heinsen, H., Thompson, P.M., Hampel, H., 2011. Staging Alzheimer's disease progression with multimodality neuroimaging. Prog Neurobiol 95, 535-546.

Fedorov, A., Beichel, R., Kalpathy-Cramer, J., Finet, J., Fillion-Robin, J.C., Pujol, S., Bauer, C., Jennings, D., Fennessy, F., Sonka, M., Buatti, J., Aylward, S., Miller, J.V., Pieper, S., Kikinis, R., 2012. 3D Slicer as an image computing platform for the Quantitative Imaging Network. Magn Reson Imaging 30, 1323-1341.

Ferrarini, L., Palm, W.M., Olofsen, H., van Buchem, M.A., Reiber, J.H., Admiraal-Behloul, F., 2006. Shape differences of the brain ventricles in Alzheimer's disease. Neuroimage 32, 1060-1069.

Fischl, B., Salat, D., Busa, E., Albert, M., Dieterich, M., Haselgrove, C., van der Kouwe, A., Killiany, R.J., Kennedy, D., Klaveness, S., Montillo, A., Makris, N., Rosen, B., Dale, A.M., 2002. Whole brain segmentation: automated labeling of neuroanatomical structures in the human brain.

Fischl, B., Salat, D.H., van der Kouwe, A.J., Makris, N., Segonne, F., Quinn, B.T., Dale, A.M., 2004. Sequence-independent segmentation of magnetic resonance images. Neuroimage 23 Suppl 1, S69-84.

Fletcher, E., 2012. See the damage. pp. Brain images published on "The Emergent Universe" web page. Images are coutesy of Evan Fletcher, IDEA Lab, UCMDC.

Fong, T.G., Jones, R.N., Marcantonio, E.R., Tommet, D., Gross, A.L., Habtemariam, D., Schmitt, E., Yap, L., Inouye, S.K., 2012. Adverse outcomes after hospitalization and delirium in persons with Alzheimer disease. Ann Intern Med 156, 848-856.

Fonov V S, N.S., Arnold D L, Collins D L, 2010. Lateral ventricle segmentation based on fusion of expert priors in AD. pp. e-poster 4255 at Joint Annual Meeting ISMRM - ESMRMB 2010.

Forstl, H., Zerfass, R., Geiger-Kabisch, C., Sattel, H., Besthorn, C., Hentschel, F., 1995. Brain atrophy in normal ageing and Alzheimer's disease. Volumetric discrimination and clinical correlations. Br J Psychiatry 167, 739-746.

Fox, N.C., Cousens, S., Scahill, R., Harvey, R.J., Rossor, M.N., 2000. Using serial registered brain magnetic resonance imaging to measure disease progression in Alzheimer disease: power calculations and estimates of sample size to detect treatment effects. Arch Neurol 57, 339-344.

Freeborough, P.A., Fox, N.C., 1997. The boundary shift integral: an accurate and robust measure of cerebral volume changes from registered repeat MRI. IEEE Trans Med Imaging 16, 623-629.

Gering, D.T., Nabavi, A., Kikinis, R., Grimson, W.E.L., Hata, N., Everett, P., Jolesz, F.A., Wells III, W.M., 1999. An Integrated Visualization System for Surgical Planning and Guidance using Image Fusion and Interventional Imaging. Int Conf Med Image Comput Comput Assist Interv. 2, 809-819.

Giesel, F.L., Hahn, H.K., Thomann, P.A., Widjaja, E., Wignall, E., von Tengg-Kobligk, H., Pantel, J., Griffiths, P.D., Peitgen, H.O., Schroder, J., Essig, M., 2006. Temporal Horn Index and Volume of Medial Temporal Lobe Atrophy Using a New Semiautomated Method for Rapid and Precise Assessment. AJNR Am J Neuroradiol 27, 1454-1458.

Gonzalez, R.C., Woods, R.E., 1992. Digital Image Processing. Addison-Wesley Publishing Company.

Gu, X.M., Jiang, Z.F., Huang, H.C., 2010. Magnetic resonance imaging of Alzheimer's disease: from diagnosis to therapeutic evaluation. Chinese Journal of Integrated Medicine 16.

Han, X., Fischl, B., 2007. Atlas renormalization for improved brain MR image segmentation across scanner platforms. IEEE Trans Med Imaging 26, 479-486.

Hattori, M., Koyama, S., Kodera, Y., 2007. [Method of segmenting inferior horns of lateral ventricles using active contour models]. Nihon Hoshasen Gijutsu Gakkai Zasshi 63, 862-870.

Hunter, J.M., Kwan, J., Malek-Ahmadi, M., Maarouf, C.L., Kokjohn, T.A., Belden, C., Sabbagh, M.N., Beach, T.G., Roher, A.E., 2012. Morphological and pathological evolution of the brain microcirculation in aging and Alzheimer's disease. PLoS One 7, e36893.

Ibanez, L., Schroeder, W., 2005. The ITK Software Guide, Second Edition. Kitware, Inc., pp. 494-497, 503-507, 520-522.

Jack, C.R., Jr., Petersen, R.C., Xu, Y.C., Waring, S.C., O'Brien, P.C., Tangalos, E.G., Smith, G.E., Ivnik, R.J., Kokmen, E., 1997. Medial temporal atrophy on MRI in normal aging and very mild Alzheimer's disease. Neurology 49, 786-794.

Jack, C.R., Jr., Shiung, M.M., Gunter, J.L., O'Brien, P.C., Weigand, S.D., Knopman, D.S., Boeve, B.F., Ivnik, R.J., Smith, G.E., Cha, R.H., Tangalos, E.G., Petersen, R.C., 2004. Comparison of different MRI brain atrophy rate measures with clinical disease progression in AD. Neurology 62, 591-600.

Jack, C.R., Jr., Shiung, M.M., Weigand, S.D., O'Brien, P.C., Gunter, J.L., Boeve, B.F., Knopman, D.S., Smith, G.E., Ivnik, R.J., Tangalos, E.G., Petersen, R.C., 2005. Brain atrophy rates predict subsequent clinical conversion in normal elderly and amnestic MCI. Neurology 65, 1227-1231.

Jack, C.R., Jr., Weigand, S.D., Shiung, M.M., Przybelski, S.A., O'Brien, P.C., Gunter, J.L., Knopman, D.S., Boeve, B.F., Smith, G.E., Petersen, R.C., 2008. Atrophy rates accelerate in amnestic mild cognitive impairment. Neurology 70, 1740-1752.

Jia H, Yap Pt, Shen, D., 2012. Iterative multi-atlas-based multi-image segmentation with tree-based registration. Neuroimage 59(1), 422-430.

Jones, T., Metaxas, D., 1997. Automated 3D segmentation using deformable models and fuzzy affinity. In: Duncan, J., Gindi, G. (Eds.), Information Processing in Medical Imaging. Springer Berlin / Heidelberg, pp. 113-126.

Kao, P.F., Banigan, M.G., Vanderburg, C.R., McKee, A.C., Polgar, P.R., Seshadri, S., Delalle, I., 2012. Increased expression of TrkB and Capzb2 accompanies preserved cognitive status in early Alzheimer disease pathology. J Neuropathol Exp Neurol 71, 654-664.

Keihaninejad, S., Heckemann, R.A., Fagiolo, G., Symms, M.R., Hajnal, J.V., Hammers, A., 2010. A robust method to estimate the intracranial volume across MRI field strengths (1.5T and 3T). Neuroimage 50, 1427-1437.

Khan, A.F., Drozd, J.J., Moreland, R.K., Borrie, M.J., Bartha, R., 2012. A novel MRI-compatible brain ventricle phantom for validation of segmentation and volumetry methods. J Magn Reson Imaging 36(2), 476-482.

Kovacevic, S., Rafii, M.S., Brewer, J.B., 2009. High-throughput, fully automated volumetry for prediction of MMSE and CDR decline in mild cognitive impairment. Alzheimer Dis Assoc Disord 23, 139-145.

Krishnapuram, R., Keller, J.M., 1993. A Possibilistic Approach to Clustering. IEEE Transactions on Fuzzy Systems 1, 98-110.

Leinsinger, G., Teipel, S., Wismuller, A., Born, C., Meindl, T., Flatz, W., Schonberg, S., Pruessner, J., Hampel, H., Reiser, M., 2003. [Volumetric MRI for evaluation of regional pattern and progressin of neocortical degeneration in Alzheimer's disease]. Radiologe 43, 537-542.

Lim, J.S., 1990. Two-Dimensional Signal and Image Processing. Prentice Hall, Inc.

Logue, M.W., Posner, H., Green, R.C., Moline, M., Cupples, L.A., Lunetta, K.L., Zou, H., Hurt, S.W., Farrer, L.A., Decarli, C., 2011. Magnetic resonance imaging-measured atrophy and its relationship to cognitive functioning in vascular dementia and Alzheimer's disease patients. Alzheimers and Dementia 7.

Macdonald, K.E., Bartlett, J.W., Leung, K.K., Ourselin, S., Barnes, J., 2012. The Value of Hippocampal and Temporal Horn Volumes and Rates of Change in Predicting Future Conversion to AD. Alzheimer Dis Assoc Disord.

Mahanand, B.S., Suresh, S., Sundararajan, N., Aswatha Kumar, M., 2012. Identification of brain regions responsible for Alzheimer's disease using a Self-adaptive Resource Allocation Network. Neural Netw 32, 313-322.

McLachlan, G.J., Krishnan, T., 1997. The EM Algorithm and Extensions. John Wiley and Sons, Inc.

Meiner, Z., Rosenmann, H., 2012. [Biological markers in the diagnosis of dementia and Alzheimer's disease]. Harefuah 151, 289-293, 318.

Mendez, M.F., Lee, A.S., Joshi, A., Shapira, J.S., 2012. Nonamnestic presentations of early-onset Alzheimer's disease. Am J Alzheimers Dis Other Demen 27, 413-420.

Mori, T., Maeda, J., Shimada, H., Higuchi, M., Shinotoh, H., Ueno, S., Suhara, T., 2012. Molecular imaging of dementia. Psychogeriatrics 12, 106-114.

Mu, Q., Xie, J., Wen, Z., Weng, Y., Shuyun, Z., 1999. A quantitative MR study of the hippocampal formation, the amygdala, and the temporal horn of the lateral ventricle in healthy subjects 40 to 90 years of age. Ajnr: American Journal of Neuroradiology 20, 207-211.

Murphy, D.G., DeCarli, C.D., Daly, E., Gillette, J.A., McIntosh, A.R., Haxby, J.V., Teichberg, D., Schapiro, M.B., Rapoport, S.I., Horwitz, B., 1993. Volumetric magnetic resonance imaging in men with dementia of the Alzheimer type: correlations with disease severity. Biol Psychiatry 34, 612-621.

Nestor, S.M., Gibson, E., Gao, F.Q., Kiss, A., Black, S.E., for the Alzheimer's Disease Neuroimaging, I., 2012. A direct morphometric comparison of five labeling protocols for multi-atlas driven automatic segmentation of the hippocampus in Alzheimer's disease. Neuroimage 66C, 50-70.

Nestor, S.M., Rupsingh, R., Borrie, M., Smith, M., Accomazzi, V., Wells, J.L., Fogarty, J., Bartha, R., Initi, A.s.D.N., 2008. Ventricular enlargement as a possible measure of Alzheimers disease progression validated using the Alzheimers disease neuroimaging initiative database. Brain 131, 2443-2454.

Ott, B.R., Cohen, R.A., Gongvatana, A., Okonkwo, O.C., Johanson, C.E., Stopa, E.G., Donahue, J.E., Silverberg, G.D., Alzheimer's Disease Neuroimaging, I., 2010. Brain ventricular volume and cerebrospinal fluid biomarkers of Alzheimer's disease. J Alzheimers Dis 20, 647-657.

Perona, P., Malik, J., 1990. Scale-Space and Edge Detection Using Anisotropic Diffusion. IEEE Trans. Pattern Analysis and Machine Intelligence 12, 629-639.

Petersen, R.C., Jack, C.R., Jr., Xu, Y.C., Waring, S.C., O'Brien, P.C., Smith, G.E., Ivnik, R.J., Tangalos, E.G., Boeve, B.F., Kokmen, E., 2000. Memory and MRI-based hippocampal volumes in aging and AD. Neurology 54, 581-587.

Pieper, S., Halle, M., Kikinis, R., 2004. 3D SLICER. Proceedings of the 1st IEEE International Symposium on Biomedical Imaging: From Nano to Macro 1, 632-635.

Pieper, S., Lorensen , B., Schroeder, W., Kikinis, R., 2006. The NA-MIC Kit: ITK, VTK, Pipelines, Grids and 3D Slicer as an Open Platform for the Medical Image Computing Community. Proceedings of the 3rd IEEE International Symposium on Biomedical Imaging: From Nano to Macro 1, 698-701.

Pohl, K.M., Bouix, S., Nakamura, M., Rohlfing, T., McCarley, R.W., Kikinis, R., Grimson, W.E.L., Shenton, M.E., Wells, W.M., 2007. A Hierarchical Algorithm for MR Brain Image Parcellation. IEEE Trans Med Imaging 26, 1201-1212.

Pohl, K.M., Fisher, J., Grimson, E.L., Kikinis, R., Wells, W.M., 2006. A Bayesian model for joint segmentation and registration Neuroimage 31, 228-239.

Preboske, G.M., Gunter, J.L., Ward, C.P., Jack, C.R., Jr., 2006. Common MRI acquisition non-idealities significantly impact the output of the boundary shift integral method of measuring brain atrophy on serial MRI. Neuroimage 30, 1196-1202.

Qiu, A., Fennema-Notestine, C., Dale, A.M., Miller, M.I., 2009. Regional shape abnormalities in mild cognitive impairment and Alzheimer's disease. Neuroimage 45, 656-661.

Saha, P.K., Udupa, J.K., 2001. Fuzzy connected object delineation: Axiomatic path strength definition and the case of multiple seeds. Computer Vision and Image Understanding 83, 275-295.

Sanchez-Benavides, G., Gomez-Anson, B., Sainz, A., Vives, Y., Delfino, M., Pena-Casanova, J., 2010. Manual validation of FreeSurfer's automated hippocampal segmentation in normal aging, mild cognitive impairment, and Alzheimer Disease subjects. Psychiatry Res 181, 219-225.

Schott, J.M., Price, S.L., Frost, C., Whitwell, J.L., Rossor, M.N., Fox, N.C., 2005. Measuring atrophy in Alzheimer disease: a serial MRI study over 6 and 12 months. Neurology 65, 119-124.

Segonne, F., Dale, A.M., Busa, E., Glessner, M., Salat, D., Hahn, H.K., Fischl, B., 2004. A hybrid approach to the skull stripping problem in MRI. Neuroimage 22, 1060-1075.

Silbert, L.C., Quinn, J.F., Moore, M.M., Corbridge, E., Ball, M.J., Murdoch, G., Sexton, G., Kaye, J.A., 2003. Changes in premorbid brain volume predict Alzheimer's disease pathology. Neurology 61, 487-492.

Smith, C.D., Andersen, A.H., Gold, B.T., 2012. Structural Brain Alterations before Mild Cognitive Impairment in ADNI: Validation of Volume Loss in a Predefined Antero-Temporal Region. J Alzheimers Dis.

Smith, S.M., Rao, A., De Stefano, N., Jenkinson, M., Schott, J.M., Matthews, P.M., Fox, N.C., 2007. Longitudinal and cross-sectional analysis of atrophy in Alzheimer's disease: cross-validation of BSI, SIENA and SIENAX. Neuroimage 36, 1200-1206.

Suzman, R., Beard, J., 2011. Global Health and Aging. In: National Institute on Aging, N.I.o.H., U.S. Departmant of Health and Human Services, World Health Organization (Ed.). NIH, p. 14.

Tanabe, J.L., Amend, D., Schuff, N., DiSclafani, V., Ezekiel, F., Norman, D., Fein, G., Weiner, M.W., 1997. Tissue segmentation of the brain in Alzheimer disease. AJNR Am J Neuroradiol 18, 115-123.

Teipel, S.J., Peters, O., Heuser, I., F., J., Maier, W., Froelich, L., Arlt, S., Hull, M., Gertz, H.J., Kornhuber, J., Wiltfang, J., Thome, J., Rienhoff, O., Meindl, T., Hampel, H., Grothe, M., 2011. Atrophy outcomes in multicentre clinical trials on Alzheimer's disease: effect of different processing and analysis approaches on sample sizes. World Journal of Biological Psychiatry 12 Supplement 1.

Ter Romeney, B.M., 1994. Geometry-Driven Diffusion in Computer Vision. Kluwer Academic Publishers, Dordrecht, The Netherlands.

Thompson, P.M., Hayashi, K.M., De Zubicaray, G.I., Janke, A.L., Rose, S.E., Semple, J., Hong, M.S., Herman, D.H., Gravano, D., Doddrell, D.M., Toga, A.W., 2004. Mapping hippocampal and ventricular change in Alzheimer disease. Neuroimage 22, 1754-1766.

Tohka, J., Zijdenbos, A., Evans, A., 2004. Fast and robust parameter estimation for statistical partial volume models in brain MRI. Neuroimage 23, 84-97.

Udupa, J.K., Saha, P.K., 2003. Fuzzy connectedness and image segmentation. Proceedings of the Ieee 91, 1649-1669.

Udupa, J.K., Samarasekera, S., 1995. Fuzzy Connectedness and Object Definition. Image Display - Medical Imaging 1995 2431, 2-11

638.

Vellas, B., Hausner, L., Frolich, L., Cantet, C., Gardette, V., Reynish, E., Gillette, S., Ag Era-Morales, E., Auriacombe, S., Boada-Rovira, M., Bullock, R., Byrne, J., Cherubini, A., Eriksdotter, J.N.M., Frisoni, G., Hasselbalch, S., Jones, R., Martinez-Lage, P., Rikkert, M., Tsolaki, M., Ousset, P.J., Pasquier, F., Ribera-Casado, J.M., Rigaud, A.S., Robert, P., Rodriguez, G., Salmon, E., A, S., Scheltens, P., Schneider, A., Spiru, L., Touchon, J., Zekry, D., Winblad, B., Andrieu, S., 2012. Progression of Alzheimer disease in Europe: Data from the European ICTUS study. Curr Alzheimer Res.

Vercauteren, T., Pennec, X., Malis, E., Perchant, A., Ayache, N., 2007a. Insight into efficient image registration techniques and the demons algorithm. Inf Process Med Imaging 20, 495-506.

Vercauteren, T., Pennec, X., Perchant, A., Ayache, N., 2007b. Non-parametric diffeomorphic image registration with the demons algorithm. Med Image Comput Comput Assist Interv 10, 319-326.

Wang, D., Chalk, J.B., Rose, S.E., de Zubicaray, G., Cowin, G., Galloway, G.J., Barnes, D., Spooner, D., Doddrell, D.M., Semple, J., 2002. MR image-based measurement of rates of change in volumes of brain structures. Part II: application to a study of Alzheimer's disease and normal aging. Magn Reson Imaging 20, 41-48.

Wang, H., Das, S.R., Suh, J.W., Altinay, M., Pluta, J., Craige, C., Avants, B., Yushkevich, P.A., Alzheimer's Disease Neuroimaging, I., 2011. A learning-based wrapper method to correct systematic errors in automatic image segmentation: consistently improved performance in hippocampus, cortex and brain segmentation. Neuroimage 55, 968-985.

Whitwell, J.L., Jack, C.R., Jr., Pankratz, V.S., Parisi, J.E., Knopman, D.S., Boeve, B.F., Petersen, R.C., Dickson, D.W., Josephs, K.A., 2008. Rates of brain atrophy over time in autopsy-proven frontotemporal dementia and Alzheimer disease. Neuroimage 39, 1034-1040.

Yamashita, F., Sasaki, M., Takahashi, S., Matsuda, H., Kudo, K., Narumi, S., Terayama, Y., Asada, T., 2010. Detection of changes in cerebrospinal fluid space in idiopathic normal pressure hydrocephalus using voxel-based morphometry. Neuroradiology 52, 381-386.

Yoo, T.S., Ackerman, M.J., Lorensen, W.E., Schroeder, W., Chalana, V., Aylward, S., Metaxas, D., Whitaker, R., 2002. Engineering and algorithm design for an image processing Api: a technical report on ITK--the Insight Toolkit. Stud Health Technol Inform. 85, 586-592.